Journal of Power Sources 221 (2013) 272–283

Contents lists available at SciVerse ScienceDirect

Journal of Power Sources

journal homepage: www.elsevier.com/locate/jpowsour

Modeling a hybrid Rankine-cycle/fuel-cell underwater propulsion system based on aluminum–water combustion

Daniel F. Waters, Christopher P. Cadou*

Department of Aerospace Engineering, University of Maryland, 3179D Glenn L. Martin Hall, College Park, MD 20740, USA

HIGHLIGHTS

- Underwater propulsion using aluminum–water combustion for high energy density.
- Included SOFC for eliminating H_2 venting, improved efficiency, depth independence.
- Developed scaling methods to link thermodynamics to system energy density.
- 2.5- to 7-fold range improvement over batteries with aluminum combustor system.
- 3- to 4-fold improvement over batteries (and no H_2 venting) when SOFC is added.

ARTICLE INFO

Article history:
Received 13 June 2012
Received in revised form
26 July 2012
Accepted 30 July 2012
Available online 11 August 2012

Keywords:
Modeling
Fuel cell
Solid oxide
Aluminum
Underwater
UUV

ABSTRACT

This work investigates the integration of solid oxide fuel cells with a novel underwater propulsion system based on the exothermic reaction of aluminum with seawater. The purpose of the fuel cell is to increase the overall thermodynamic efficiency of the system and consume waste hydrogen produced by the aluminum–water reaction. The system is modeled using a NASA-developed framework, Numerical Propulsion System Simulation, by assembling thermodynamic models of components. The base aluminum–water system can increase range/endurance by factors of 2.5–7 over equivalent battery powered systems. Incorporating the fuel cell may not be beneficial when venting hydrogen overboard is permissible. However, when venting hydrogen is not permissible – which would be the situation for most naval underwater missions – the fuel cell is essential for consuming waste hydrogen and the combined combustor/fuel cell system provides a 3–4 fold increase in range/endurance compared to batteries. Methodologies for predicting how component volumes scale with power are developed to enable prediction of power and energy density. The energy density of the system is most sensitive to the efficiencies of the turbine and H_2 compressor. The ability to develop a compact and efficient isothermal hydrogen compressor is also critical to maximizing performance.

1. Introduction

The United States Navy has a growing need for advanced Unmanned Undersea Vehicles (UUVs) that can complete critical missions while keeping sailors out of harm's way. Several key naval missions including intelligence, surveillance, and reconnaissance have been identified as best performed by UUVs [1]. Underwater power and energy systems that maximize vehicle range and endurance while minimizing detectability are critical to the success of all of these missions.

1.1. Range and endurance

The range and endurance of a UUV cruising at constant speed (v_C) is given by [2]:

$$\text{Range} = \frac{\eta_p \cdot \text{ED}_V \cdot V_{sys}}{\left(\dot{W}_{PL}/v_C\right) + \left(\frac{1}{2}\rho_{seawater} v_C^2\right) \cdot (C_D A_{cross})} \quad (1)$$

$$\text{Endurance} = \Delta t = \frac{\eta_p \cdot \text{ED}_V \cdot V_{sys}}{\dot{W}_{PL} + \left(\frac{1}{2}\rho_{seawater} v_C^3\right) \cdot (C_D A_{cross})} \quad (2)$$

In these expressions, $\dot{W}_{PL}$ is the payload power, C_D is the vehicle drag coefficient, A_{cross} is the vehicle cross-section area, η_p is the

* Corresponding author. Tel.: +1 301 405 0829; fax: +1 301 314 9001.
E-mail address: cadou@umd.edu (C.P. Cadou).

0378-7753/$ – see front matter © 2012 Elsevier B.V. All rights reserved.
http://dx.doi.org/10.1016/j.jpowsour.2012.07.085

propulsive efficiency, V_{sys} is the total volume of the power and energy system, and ED_V is the 'effective' energy density of the power and energy system. The 'effective' energy density is the total recoverable energy available in the system divided by the total system volume (conversion system plus fuel). It is given by:

$$ED_V = \eta_t \cdot \Delta H_{V,reac} \cdot \frac{V_{reac}}{V_{sys}} \quad (3)$$

where η_t is the thermodynamic efficiency of the power and energy system, $\Delta H_{V,reac}$ is the volumetric energy density of the fuel and V_{reac}/V_{sys} is the fraction of total system volume allocated for fuel storage. This work is concerned with evaluating the aluminum combustor/SOFC system as a 'drop in' replacement for existing power and energy systems. Therefore, V_{sys} and η_p are fixed and ED_V becomes the performance parameter of primary interest in this study. Eq. (3) shows that realizing the benefits of high energy density propellants requires devising compact and efficient energy conversion systems where the energy density of the propellant is not 'consumed' by the size and inefficiency of the conversion system.

1.2. Stealth

Since many Navy missions require stealth, a propulsion system's detectability can be at least as important as its range and endurance. Many factors contribute to a vehicle's ability to avoid detection. These include its acoustic, magnetic, electric, and pressure signatures [1], its external reflective properties (radar cross-section), and any physical/chemical trails left behind in the water through which it travels. Noise generation (acoustic signature) is unavoidable in conventional propeller-driven undersea vehicles although it can be reduced through careful hydrodynamic design and the use of sound absorbing materials. Any detectable trail left by the vehicle would also be a significant problem. A primary concern is buoyant waste products vented or dumped from the vehicle that could rise to the surface leaving an easily visible and traceable path. Another concern is invisible but chemically detectable traces left in the water like elevated Al_2O_3 or H_2 concentrations.

1.3. UUV power/energy options

At present, the US Navy primarily utilizes two forms of underwater propulsion. The first is Otto fuel driven heat engines used by torpedoes like the Mk48. Otto fuel is a relatively stable liquid monopropellant which rapidly decomposes into hot gaseous products when ignited [3]. It is very effective for the torpedo's high power, short endurance mission but is not well suited for UUVs whose missions require much less propulsive power (because they travel at much lower speeds), much more electrical power for guidance, sensors, etc., must start and stop frequently, and have a need for 'stealth'. As a result, the current fleet of UUVs is battery-powered [1]. This means its range and endurance are relatively limited because the energy densities of state-of-the-art batteries are relatively low. Batteries also have long turn-around times associated with replacement and/or recharging after every mission. However, despite a battery's low ΔH_V, its conversion efficiency is very high (>95% if discharged at an adequately low rate) and the volume of the conversion system is negligible compared to the volume of the energy storage material. These factors combined with a battery's simplicity, silence, and ability to turn on and off instantly make it very attractive in underwater systems.

There have been attempts over the years to construct systems that could supplant batteries. These efforts have investigated various types of fuel cells (including solid-oxide [4], direct boro-hydride [5], etc.) as well as strategies for storing energy dense reactants like hydrocarbon fuels [4], oxygen-dense compounds [6], and cryogenic liquid O_2 [7]. The lower portion of Table 1 shows energy densities of 'conventional' fuel and oxidizer systems as well as Otto fuel [3] and batteries [5,8,9]. Air is excluded as an oxidizer because it is not available in the underwater environment. H_2 and O_2 are assumed to be stored in their liquid states. The data show that the overwhelming energy density advantage enjoyed by liquid hydrocarbons in air-breathing systems disappears entirely when oxidizer must be included in the propellant mass/volume.

A promising alternative to battery-based energy storage that has been investigated since the early 1960s is metals that react exothermically with seawater [3]. Such systems offer advantages similar to those enjoyed by air-breathing engines where the oxidizer is harvested from the vehicle's surroundings and does not need to be stored on board. Many metals have been investigated over the years including aluminum [10] and lithium [11]. The top portion of Table 1 summarizes the energy content of various metal fuel/oxidizer systems. Other high energy density propellant combinations like boron-water and beryllium-water are excluded from the list for reasons of cost and/or toxicity [12]. Unlike aircraft where lift-induced drag makes vehicle weight a key restriction, underwater vehicles are primarily influenced by skin drag and form drag (both heavily dependent on the vehicle's physical dimensions) [13]. Therefore, energy content on a 'per volume' basis is the primary consideration for the underwater environment. The lithium–water reaction rates highly on a 'per mass' basis, but the low density of lithium results in poor 'per volume' performance. Similarly, combinations with hydrogen fuel have high 'per mass' energy content but are not ideally suited for underwater use because of hydrogen's extremely low density (even in liquid form).

Table 1 shows that the aluminum–water reaction (Eq. (4)) provides the largest heat release per unit volume and therefore is most suitable for underwater applications.

$$2Al + 3H_2O \rightarrow Al_2O_3 + 3H_2; \quad \Delta H = -409\ kJ/mol_{AL} \quad (4)$$

The energy content of this reaction relative to batteries suggests that improvements in range/endurance of an order of magnitude or more are thermodynamically possible provided suitably compact and efficient energy conversion systems can be devised.

Table 1
Energy content of various undersea reactant combinations.

Fuel	Oxidizer	Specific energy (W h kg^{-1})	Energy density, ΔH_V (W h L^{-1})
Al	H_2O	4212	11,374
Zr	H_2O	1611	10,503
Al	$LiClO_4$	3523	8898
Mg	H_2O	3609	6273
Li	H_2O	7969	4256
H_2	O_2	3728	1535
H_2	H_2O_2	2280	1551
C_XH_Y	O_2	2730–2790	2300–2800
C_XH_Y	H_2O_2	1840–1870	2100–2500
$NaBH_4$	O_2	3470	3869
$NaBH_4$	H_2O_2	2377	3224
CH_3OH	O_2	2214	2147
Otto fuel [3]		705	895
Li-ion batteries [5,8]		90–130	180–315
Alkaline batteries [9]		110–200	150–270
Pb-acid batteries [9]		70–120	30–60

A Rankine cycle system based on the combustion of powdered aluminum with seawater called the Hybrid Aluminum Combustor (HAC) has been proposed by Kiely et al. [10,14]. Its thermodynamic viability [15,16] and potential effective energy density [2,17] were investigated by Eagle et al. and Waters. The results showed that the system's thermodynamic efficiency was comparable to other similarly-sized heat engines and that large increases in effective energy density and hence range and endurance were possible over battery-powered systems. However, an important problem was the large volume of waste H_2 gas produced by the Al–H_2O reaction: Venting this gas overboard could be unacceptable for reasons of stealth but the large thermodynamic cost of compressing and storing the waste gas on board is unacceptable for maintaining acceptable effective energy density.

Therefore, the objective of the current work is to investigate the use of solid oxide fuel cells (SOFCs) as a means for converting the waste H_2 to water that can be stored on board more easily or released overboard unobtrusively. Another advantage of incorporating the SOFCs is that they are more thermodynamically efficient than the Rankine cycle and so could raise the effective energy density of the system.

1.4. Propulsion system concept

Fig. 1 is a schematic illustration of the aluminum–water powered Rankine cycle system (HAC) with integrated SOFC. The system is similar to the one studied earlier by Eagle [15,16] except that a SOFC sits between the turbine and recuperator. The addition of the SOFC has a minimal effect on the operation of the HAC portion of the system as it only changes the temperature and composition of the hot side recuperator flow. The system operates as follows [2,16]: The high pressure fuel system, or fuel "seeder", produces a stream of aluminum powder suspended in a small flow of H_2 which feeds a pre-combustor where it reacts in stoichiometric proportions with steam to form aluminum oxide (also known as alumina), more H_2, and heat as in Eq. (4). Quenching water is injected around the internal circumference of the combustor to produce large amounts of steam and to solidify the molten alumina before it is able to stick to the walls. Developing an injection system that prevents slagging is an important engineering challenge in aluminum burning systems [18] that has been largely solved by researchers at Pennsylvania State University [10]. The flow then passes through a separator to remove the solidified alumina. The remaining flow is diverted into two streams. A small portion (20–25% depending on operating condition) is recirculated to provide the superheated steam that initiates the reaction in the combustor. The remainder passes through a turbine that extracts mechanical power for the vehicle. The flow exiting the turbine passes through the SOFC where a fraction of the hydrogen is consumed to produce electric power. This fraction is termed the 'H_2 utilization'. The flow then passes to a heat exchanger that uses waste enthalpy in the exhaust to pre-warm the quenching water thereby improving overall efficiency. The remaining steam is fully condensed to liquid water and supplemented with seawater to make up for what was consumed by the reaction. A portion of the hydrogen gas is separated from the condensed water, compressed, and reused for aluminum "seeding". Any *remaining* H_2 must be vented overboard or compressed and stored. The hydrogen may be compressed either adiabatically or isothermally.

While incorporating a fuel cell that consumes hydrogen enables one to mitigate the problem of excess hydrogen, it requires the following additional components: an oxidizer tank (63% by mass H_2O_2), a membrane electrode assembly (MEA), a condenser and separator to trap and remove the water produced in the MEA, and a compressor to return unused O_2 to the cathode. A decomposition reactor is also added to facilitate the breakdown of H_2O_2 to H_2O and O_2 although it could be possible to do this directly on the SOFC's cathode. The key question is whether or not these additional components (which displace aluminum fuel) increase or decrease system-level energy density when the work associated with compressing the H_2 (either to store it or discharge it overboard) is accounted for.

1.5. Isothermal compression

In many applications it is not practical to consider isothermal compression because of the large amount of heat that must be removed but the ready availability of cooling water makes this

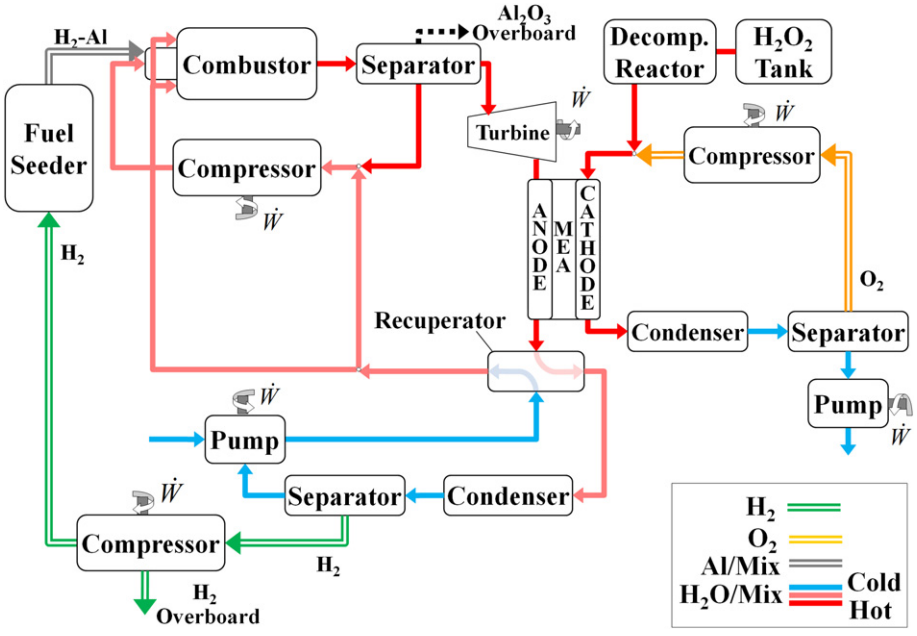

Fig. 1. HAC-SOFC hybrid system diagram.

a more practical option underwater where the heat exchangers could be much smaller and potentially even integrated into the hull. A simple thermodynamic analysis of a perfectly intercooled 3-stage hydrogen compressor – i.e., one where the exhaust temperature is returned to the inlet temperature before entering the next stage – achieves over 75% of the benefit of isothermal compression: $(\dot{W}_{\text{adiabatic}} - \dot{W}_{\text{staged}})/(\dot{W}_{\text{adiabatic}} - \dot{W}_{\text{isothermal}}) > 0.75$ [19,20]. This improves to greater than 85% with 5 perfectly intercooled stages. However, the extra compressor stages and heat exchangers consume additional volume that displaces fuel and could reduce overall system energy density. Which compression mode is best depends on the degree of improvement in compression efficiency compared to the associated increase in volume. Such a detailed trade study of the compressor is beyond the scope of this work so the approach taken here is to identify the limits of system performance associated with adiabatic vs. isothermal compression and then to show how the isothermal limit shifts as a function of the additional volume required to achieve isothermal compression.

2. Model formulation

2.1. Simulation environment

Mathematical models are developed for each component of the system. Each model has inputs, outputs, and parameters that control the operation of the component. The condition of the flow at any point in the system is described by the mass flow, pressure, temperature, and composition (i.e., the mass fractions of H_2, Al, etc.). The system can be solved by treating each component as a matrix that operates on the incoming state space vector but convergence can be difficult in systems like these that have multiple feedback loops and many components whose input–output relationships are highly nonlinear.

Instead, a software package called Numerical Propulsion System Simulation (NPSS) [21] is used to create and solve the system. While NPSS was intended to be a generalized design and analysis tool for developing gas turbine engines, it is well-suited for investigations of other systems like the one of interest here. The principal advantage of NPSS is that it handles the mathematical difficulties associated with solving recursively-coupled systems of nonlinear equations thus enabling the user to focus on developing appropriate component models. It has built-in data structures that facilitate the transfer of information between components and a solver for finding the state points of the system. Other advantages of NPSS include extensive libraries of predefined components, the ability to easily develop new components, and a high degree of flexibility in the types of component models that can be used with it. For example, it is possible to represent a component using a model written in C++ (this is mostly what is done here), a lookup table relating inputs to outputs, or by linking to complex external simulation programs like CHEMKIN or FLUENT®. NPSS also allows the user to choose among several thermodynamic calculation methods including gas table lookup and full chemical equilibrium calculations using CEA [22].

The NPSS solver allows the user to define independent variables and dependent conditions. The number of independent variables and dependent conditions must be equal. The solver perturbs the values of the independent variables to form a Jacobian matrix. Then, a modified Newton–Rhapson method [21] is used to adjust the values of the independent variables in order to drive the error in the dependent conditions to zero. A major challenge is that the solver will diverge if initial conditions are selected that are not close enough to the converged solution. This problem is overcome here by starting with a single known initial state that produces a converged solution and then gradually varying parameters away from the known state using the most recent converged solution as the new initial condition. Additional information about the solver and how it works can be found elsewhere [21].

2.2. Hybrid HAC-SOFC system model

Previous work by Eagle et al. [15,16] and Waters [2,17] developed a thermodynamic model in NPSS and volume scaling methods for energy density calculations for a baseline HAC system. The current work expands this model by incorporating models for a SOFC and its associated components. The analysis focuses on the design of a 1000 L power section which is consistent with a vehicle on the lower end of the large class UUV range as defined by the Navy [1,23]. The analysis also applies to vehicles larger than the 21″ diameter class [24].

The NPSS model of the HAC-SOFC system is illustrated in Fig. 2. It has been designed to correspond directly to the physical system schematic in Fig. 1. A small difference is the addition of three numerical 'Loop' elements. These elements are necessary for solving this complex system with multiple recursive flow loops. For example, the flow state exiting the combustor depends on itself through the steam recirculation pathway. The 'Loop' element provides initial approximations of temperature, pressure, mass flow rate, and composition that enable the solver to proceed to a solution. In the unconverged state, the inlet and outlet states of these elements will be mismatched causing flow properties to undergo step changes that are non-physical. One of the requirements for a converged solution is that the inlet and outlet states be identical. The other difference to note is the absence of a separate H_2O_2 decomposition reactor in the NPSS model. This component is not needed because the process is modeled automatically at the 'MixStart' oxidizer exit flow station using a CEA calculation that determines the equilibrium composition and temperature for a constant enthalpy process.

The NPSS model is used to compute pressures, temperatures, and flow rates throughout the system at various operating conditions. It also computes the power consumption of compressors and power production of turbines to find the net system power. The simulation results are combined with some scaling rules for heat exchangers [2] that are used to size the HAC and SOFC. This in turn allows one to estimate how the volumetric energy density varies with operating condition so that the optimal operating points may be identified.

The following sections describe the mathematical models used to represent the components added to the baseline HAC system to represent the SOFC and to estimate component volumes. The reader is referred elsewhere [2,15–17] for descriptions of the mathematical models used to represent the baseline HAC system.

2.3. Model operating cases

The first run of the HAC-SOFC model is with the H_2 utilization rate $(= \dot{m}_{H_2,\text{reacted}}/\dot{m}_{H_2,\text{inlet}})$ set to 0%. This corresponds to the case where the fuel cell is off or, equivalently, the baseline HAC system is operating without a fuel cell. This case was used to check the model and the results are identical to those obtained in earlier investigations of the HAC system without a fuel cell [15]. This first run also provides the starting point for all future calculations. The full range of available H_2 utilizations is examined from 0% up to 53% where all of the 'excess' H_2 is consumed. The remaining 47% of the H_2 produced by the Al–H_2O reaction is needed to operate the aluminum seeder. Two "cases" are investigated:

A. "H_2 venting": The work required to compress all excess H_2 to the ambient (local depth) pressure in order to be dumped overboard is accounted for when computing the net power

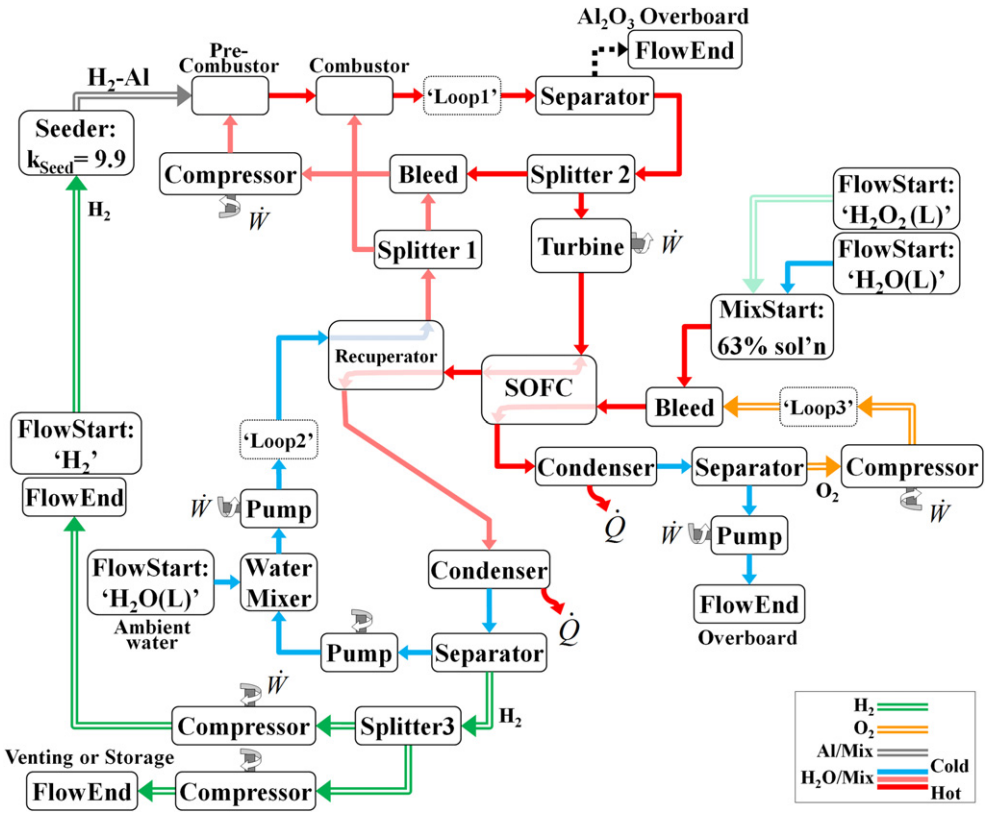

Fig. 2. NPSS model of the HAC-SOFC hybrid system.

output of the system. Depths of 3 m (131.7 kPa), 30 m (407.5 kPa), and 150 m (1633.4 kPa) are investigated to cover the operating range defined as necessary by the Navy for UUVs in this class [23,24]. No volume is allocated for H_2 storage.

B. "H_2 storage": The work required to compress all excess H_2 to a specified pressure (6900 kPa) in order to be stored on board is accounted for when computing the power output of the system. The final volume of the stored H_2 is accounted for in the energy density calculations.

Calculations for each case begin at 0% H_2 utilization and 15 kW net power output. This power level is chosen in order to be consistent with a 1000 L power section operating at 10–20 W L^{-1} power density [24]. The HAC system is scaled as required by varying the fuel mass flow (which in turn causes other flows in the system to vary). The NPSS model is run for a series of incrementally higher H_2 utilizations up to 53%. In Case A, the power output of the system remains constant at each iteration. Case B is more complex because the parasitic power associated with H_2 storage gets progressively larger as the storage tank fills and its pressure rises. This means that that the gross power output of the system must increase over the course of the mission in order to maintain the 15 kW net power to drive the vehicle. Therefore, the energy density of the Case B system is computed with the system in its final state (H_2 at 6900 kPa in the storage tank and 15 kW net power. The efficiencies of all components are assumed to remain constant over the duration of the mission. The effects of adiabatic vs. isothermal hydrogen compression are also examined to demonstrate lower and upper performance bounds, respectively.

2.4. Solid oxide fuel cell model

The overall reaction occurring in the SOFC system is $H_2 + 1/2O_2 \rightarrow H_2O$. The model for mass transport across the MEA is based on an existing SOFC element developed at the University of California–Irvine[1] while the electrochemical model is based on work done at the University of Maryland and the Colorado School of Mines [25–28]. The parameters for the electrochemical modeling are summarized in Table 2. The detailed chemical kinetics of the process are not modeled. Instead, the H_2 utilization rate – which is the fraction of the hydrogen gas in the anode flow that is consumed by the chemical reaction – is treated like a parameter and varied. When a certain fraction of H_2 is removed from the anode flow, an equal number of moles of H_2O are added to the anode flow and one half this number of moles of O_2 is removed from the cathode side flow [29]. The size of the SOFC is adjusted to ensure that the cell active area is consistent with the current density and total current in the cell.

An energy balance is performed to determine the operating temperature of the fuel cell. This is accomplished by adjusting temperature as an independent variable to satisfy the condition that the energy converted to electricity is equal to the difference in enthalpy between the inlet and outlet plus the heat transfer to the system, $\dot{W}_{SOFC} = (\dot{m}_{in} \cdot h_{in} - \dot{m}_{out} \cdot h_{out}) + \dot{Q}$. The SOFC is assumed to be adiabatic ($\dot{Q} = 0$) and the entire MEA is assumed to be at a uniform temperature. A higher fidelity model would need to account for heat losses and local temperature variations within the SOFC, but because the temperatures of both anode and cathode flows (typically 1000–1100 K and 800–850 K, respectively) entering the cell are near to or within the range of the cell's final operating temperature (roughly 1000–1400 K, depending on operating conditions), it is reasonable to assume that spatial temperature gradients within the flow are relatively small.

[1] Pratt, J., NPSS modeling, University of California–Irvine NFCRC, via e-mail Correspondence with Tom Lavelle, 2008.

Table 2
Fuel cell model parameters.

Parameter	Value	Units
Anode		
Thickness, δ_a	30	μm
Porosity, ϕ	0.3	
Tortuosity, τ	6	
Symmetry factors, $\alpha_{a,f}\alpha_{a,r}$	1.5, 0.5	
Apparent activation energy, E_{a,H_2}	120	kJ mol^{-1}
Exchange current factor, $i^*_{H_2,ref}$	4.25	A cm^{-2}
Desorption pre-exponential, A_{des}	5.59×10^{15}	m^2 mol^{-1} s^{-1}
Desorption activation energy, $E_{a,des}$	88.12	kJ mol^{-1}
Surface site density, Γ	2.6×10^{-5}	mol m^{-2}
Sticking probability, γ_0	0.01	
Cathode		
Thickness, δ_c	50	μm
Porosity, ϕ	0.3	
Tortuosity, τ	5	
Symmetry factors, $\alpha_{c,f}$, $\alpha_{c,r}$	1.5, 0.5	
Apparent activation energy, E_{a,O_2}	130	kJ mol^{-1}
Exchange current factor, $i^*_{O_2,ref}$	1.2	A cm^{-2}
Arrhenius pre-exponential, A_{P,O_2}	4.9×10^8	atm
Arrhenius activation energy, E_{a,P,O_2}	200	kJ mol^{-1}
Electrolyte		
Thickness, L_{elec}	30	μm
Ion conductivity, σ_0^0	3.6×10^5	K cm$^{-1}\Omega^{-1}$
Activation energy, E_a	80	kJ mol^{-1}

The fuel cell operating voltage, E_{cell}, is determined by subtracting ohmic (η_{ohm}), activation (η_{act}), and concentration (η_{con}) overpotentials from the reversible potential [25] as in Eq. (5). The reversible potential, E_{rev}, is determined using the Nernst equation (6) where ΔG^0 is the Gibbs free energy of the reaction, n is the number of electrons freed in the reaction, F is the Faraday constant, R is the universal gas constant, and P is the partial pressure of the designated species at the flow exit.

$$E_{cell} = E_{rev} - \eta_{ohm} - \eta_{act,a} - \eta_{act,c} - \eta_{con,a} - \eta_{con,c} \tag{5}$$

$$E_{rev} = -\frac{\Delta G^0}{nF} + \frac{RT}{nF}\ln\left(\frac{P_{H_2,a}\cdot P_{O_2,c}}{P_{H_2O,a}}\right) \tag{6}$$

Calculation of the overpotentials follows the work of Kee et al. [25–28]. The ohmic overpotential, Eq. (7), accounts for the voltage drop across the cell as a result of electrical resistance where L is the electrolyte thickness, i is the current density, and σ_0 is the conductivity of the electrolyte. Losses increase with temperature due to the exponential term which is also a function of an activation energy parameter, E_a.

$$\eta_{ohm} = \frac{iL}{\left[\frac{\sigma_0^0}{T}\exp\left(\frac{-E_a}{RT}\right)\right]} \tag{7}$$

The activation overpotentials at the anode and cathode account for the loss of potential resulting from the energy required to initiate chemical reaction at the anode and cathode. The calculation is based on the Butler–Volmer equation. For the anode, this is given by Eq. (8) where i_0 is the exchange current density, and $\alpha_{a,f}$ and $\alpha_{a,r}$ are symmetry parameters. Because there is no closed form expression that enables one to solve for η_{act} directly, the solver varies η_{act} as an independent variable until Eq. (8) is satisfied. Using the methods described by Zhu and Kee [26] and Zhu et al. [27], the anode exchange current is given by Eq. (9) where P^*_{H2} in Eq. (10) is a function of hydrogen adsorption and desorption rates, A_{des} is a desorption pre-exponential factor, Γ is the hydrogen surface site density, γ_0 is the hydrogen sticking probability, $E_{a,des}$ is the desorption activation energy, $i^*_{H_2,ref}$ is a reference exchange current density, and $E_{a,H2}$ is an activation energy. These parameters are usually empirically derived and are more fully described in Ref. [23]. Partial pressures are measured at the anode exit. Similarly, the activation overpotential at the cathode is found using Eqs. (11)–(13) where partial pressures are measured at the cathode exit.

$$i = i_{0,a}\left[\exp\left(\frac{\alpha_{a,f}F\eta_{act,a}}{RT}\right) - \exp\left(\frac{\alpha_{a,r}F\eta_{act,a}}{-RT}\right)\right] \tag{8}$$

$$i_{0,a} = \frac{i^*_{H_2,ref}\exp\left[-\frac{E_{a,H_2}}{R}\left(\frac{1}{T}-\frac{1}{T_{ref}}\right)\right]\left(P_{H_2}/P^*_{H_2}\right)^{1/4}\left(P_{H_2O}\right)^{3/4}}{1+\left(P_{H_2}/P^*_{H_2}\right)^{1/2}} \tag{9}$$

$$P^*_{H_2} = \frac{A_{des}\Gamma^2\sqrt{2\pi RT\cdot(MW_{H_2})}}{\gamma_0}\exp\left(-\frac{E_{a,des}}{RT}\right) \tag{10}$$

$$i = i_{0,c}\left[\exp\left(\frac{\alpha_{c,f}F\eta_{act,c}}{RT}\right) - \exp\left(\frac{\alpha_{c,r}F\eta_{act,c}}{-RT}\right)\right] \tag{11}$$

$$i_{0,c} = i^*_{O_2,ref}\exp\left[-\frac{E_{a,O_2}}{R}\left(\frac{1}{T}-\frac{1}{T_{ref}}\right)\right]\frac{\left(P_{O_2}/P^*_{O_2}\right)^{1/4}}{1+\left(P_{O_2}/P^*_{O_2}\right)^{1/2}} \tag{12}$$

$$P^*_{O_2} = A_{P,O_2}\exp\left(-\frac{E_{a,P,O_2}}{RT}\right) \tag{13}$$

Concentration overpotentials account for the loss of potential due to depletion of the supply of reactants at the reaction sites: As the reaction proceeds faster (i.e., the current density is higher), the reactants are consumed faster than they can be replaced via diffusion. Eqs. (14) and (15) give the concentration overpotentials at the anode and cathode as functions of current density and diffusion coefficients where δ is the thickness of the anode or cathode and $D_{k,eff}$ is the effective diffusion coefficient of species K in the mixture at the anode or cathode. The effective binary diffusion coefficient through the porous anode or cathode is given by Eq. (16) as a function of the porosity (ϕ) and tortuosity (τ) of the anode/cathode. While mixture averaged diffusion coefficients could be calculated for each species, binary coefficients are sufficient in this work where the anode and cathode flows only contain two gaseous species.

$$\eta_{conc,a} = -\frac{RT}{2F}\ln\left[\frac{1-\frac{RT\delta_a i}{2FD_{H_2,eff,a}P_{H_2,a}}}{1+\frac{RT\delta_a i}{2FD_{H_2O,eff,a}P_{H_2O,a}}}\right] \tag{14}$$

$$\eta_{conc,c} = -\frac{RT}{4F}\ln\left[1-\frac{RT\delta_c i\cdot(1-X_{O_2,c})}{4FD_{O_2,eff,c}P_{O_2,c}}\right] \tag{15}$$

$$D^{eff}_{KL} = \frac{\phi}{\tau}D_{KL} \tag{16}$$

2.5. Volume scaling

The volume of each component is assumed to be directly related to the flow passing through it so that components get respectively larger or smaller as the design power requirement of the system grows or shrinks. The methodology for estimating a component's size is based on the assumptions that each component is

cylindrical, flow velocity through each component is constant and uniform, and residence time through the component is constant. Based on these assumptions, the following is true:

$$V_{comp} = V_{comp,ref}\left(\frac{\dot{m}}{\dot{m}_{ref}}\right) \tag{17}$$

The mass flow rate ($\dot{m}$) used for scaling is always the total mass flow through the component. The reference states ($\dot{m}_{ref}, V_{comp,ref}$ in Table 3) are chosen to be consistent with a 15 kW output system.

While Eq. (17) works well for most components, for heat exchangers the volume will also depend on the required effectiveness. The heat exchanger is assumed to be a simple straight-tube, counter-current design. The convective heat transfer coefficient (h_Q) is assumed to be constant, the heat transfer surface area is proportional to mass flow, and the heat capacity ratio between the streams ($\dot{m}_H C_{p,H}/\dot{m}_C C_{p,C}$) is constant through the channels. By using these assumptions, an iterative finite differencing scheme was applied to model the scaling of heat exchanger length as a function of heat capacity ratio and effectiveness (ε). Based on the stated assumptions, the volume of the heat exchanger scales as:

$$V_{HE} = V_{HE,ref}\left(\frac{\dot{m}}{\dot{m}_{ref}}\right)\cdot\frac{L\left[\varepsilon,\left(\dot{m}_H C_{P,H}/\dot{m}_C C_{P,C}\right)\right]}{L\left[\varepsilon_{ref},\left(\dot{m}_H C_{P,H}/\dot{m}_C C_{P,C}\right)_{ref}\right]} \tag{18}$$

where the mass flow is the sum of the hot and cold side flows (to accurately scale the combined cross section area). Further details of this scaling process can be found in Refs. [2,17].

The fuel cell also requires a different approach to scaling than that given by Eq. (17). The NPSS model calculates the number of cells required to produce the electrical power necessary for the desired operating conditions. The calculation accounts for the total active surface area needed given the required power output and specified cell current density. This is used to estimate the volume of the stack based on prior estimates of the volume of an individual cell (0.033 L for a 64 cm^2 cell [4]) and the assumption that the SOFC system, including pipes and pumps, is 3 times the size of the stack alone [4]. Although this approach neglects additional factors that could arise in the case of a very large stack (a large stack may require proportionally more structural support and less insulation) it should provide a reasonable approximation for the size of the fuel cell stack of interest here. It is also assumed that the sizes of the pumps and piping associated with the fuel cell scale linearly with the size of the stack itself. This methodology represents a first step in estimating the SOFC's size and can be refined in future work. Based on these assumptions, the volume of the SOFC system is given by Eq. (19) where V_{SOFC}/V_{Stack} is the ratio of SOFC system volume to the volume of the stack alone (assumed scaling factor ≈ 3 here).

Table 3
System component reference states.

Component	$\dot{m}_{ref}$ (kg s^{-1})	$V_{comp,ref}$ (L)
Fuel seeder	0.0147	6.25
Combustor	0.0835	50
Oxide separator	0.0835	25
Steam compressor	0.0147	6.25
Steam turbine	0.0571	25
Heat exchanger	0.1159	62.5
Water pumps	0.0587	25
Condenser	0.0571	20
H_2 separator	0.0571	25
H_2 compressors	0.0014	5

$$V_{SOFC} = \left(\frac{V_{SOFC}}{V_{Stack}}\right)\cdot N_{cell}\cdot V_{cell} = \left(\frac{V_{SOFC}}{V_{Stack}}\right)\cdot\left(\frac{\dot{W}_{SOFC}}{\dot{W}_{cell}}\right)\cdot V_{cell} \tag{19}$$

2.6. Energy density calculations

The volume of the system is the sum of the volumes of the HAC, SOFC, reactants, and excess H_2 storage tank. To determine the volume available for reactant storage, it must be determined how the system volume is divided between these components. Based on the flow rate of reactants ($\dot{m}_{reac}$) and the flow rate of hydrogen into excess storage ($\dot{m}_{H2,Storage}$) it can be shown that:

$$\frac{V_{H_2,storage}}{V_{reac}} = \left(\frac{\rho_{eff}}{\rho_{H_2}}\right)\cdot\left(\frac{\dot{m}_{H_2,Storage}}{\dot{m}_{reac}}\right) \tag{20}$$

and for a given HAC and SOFC volume,

$$V_{reac} = \frac{V_{sys} - V_{HAC} - V_{SOFC}}{1 + \left(\frac{\rho_{eff}}{\rho_{H_2}}\right)\cdot\left(\frac{\dot{m}_{H_2,Storage}}{\dot{m}_{reax}}\right)} \tag{21}$$

where ρ_{eff} is the weighted average density of the reactants (aluminum and hydrogen peroxide). This formulation would need to change if one is interested in H_2 storage to support periods of silent operation, but without mission specific operational details, Eq. (21) provides a useful method for apportioning volume.

The volumetric energy density of the system was defined in Eq. (4). Rewriting the product of efficiency and reaction enthalpy as the ratio of system power output to reactant flow rate gives Eq. (22) for the energy density in terms of the quantities that are computed in the model.

$$ED_V = \left(\dot{W}_{HAC} + \dot{W}_{SOFC}\right)\frac{\rho_{eff}}{\dot{m}_{reac}}\frac{V_{reac}}{V_{sys}} \tag{22}$$

3. Results and discussion

3.1. Selection of current density

It is important to identify an appropriate operating state for the fuel cell when adding the SOFC to the HAC system. The key parameter under the user's control is the cell current density which, along with the incoming flow state, determines the operating state of the SOFC. Since it is prohibitive to consider all possible system operating states, the performance variation of the system as a function of current density is evaluated at a single operating point corresponding to 15 kW total system power output and 53% H_2 utilization rate (47% of the H_2 must be recycled to run the aluminum seeder). The results are presented in Fig. 3 which shows fuel cell voltage and power density as functions of current density (assuming excess H_2 is vented overboard) and Fig. 4 which shows system-level energy density vs. current density.

It is important to note that Fig. 3 is *not* directly analogous to a typical *V–I* fuel cell curve where the temperature and inlet flow compositions are held constant. In this case, the overall power output and H_2 utilization of the system are fixed. This means that the sizes of the individual components change as the current density is varied and this, in turn, changes the state of the flow exiting the turbine. For example, the cell operating temperature increases by 8% when current density increases from 0 to 1 A cm^{-2}.

At first glance, it may seem that the SOFC should operate at peak power density which would result in the smallest possible fuel cell

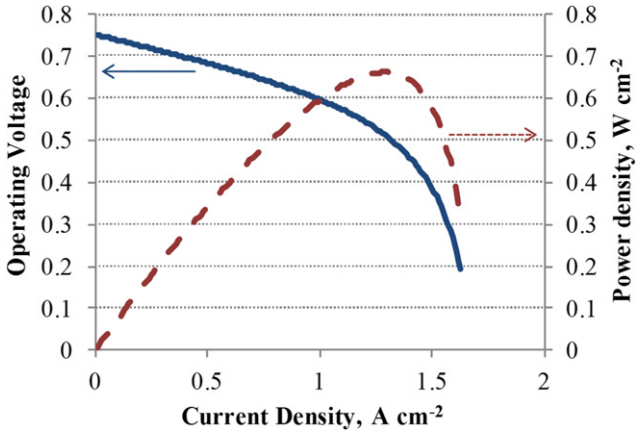

Fig. 3. Voltage and power density v. current density $\dot{W}_{NET}$ = 15 kW, H_2 ut. = 53%).

stack. However, Fig. 4 shows that the energy density of the system peaks at 0.44 A cm^{-2} which is well below the 1.4 A cm^{-2} associated with peak power density in the fuel cell. The figure assumes adiabatic compression, but the trend is the same for an isothermal process. The reasons for the peak below 1.4 A cm^{-2} are as follows: At very low current density, the SOFC voltage is high but the system energy density is low because the SOFC stack must be large to meet the power requirement and displaces a lot of fuel. Increasing the current density reduces the size of the SOFC leaving more room for fuel, but it also decreases the cell voltage and thereby decreases the cell efficiency. As a result, doubling the current density does not double the power output, and the fuel cell's contribution to the total system power decreases with increasing current density (when the H_2 utilization is held constant). Thus, the HAC system must grow in order to maintain constant system power. Initially, trading cell voltage and increased HAC size for decreased SOFC stack size is favorable from an 'effective' energy density point of view. However, at larger power densities, the increased size of the HAC required to offset the loss of SOFC power more than negates the benefit of using a smaller stack. The peak at 0.44 A cm^{-2} in Fig. 4 represents the best compromise between these effects for H_2 utilization of 53%.

Finally, it is also important to note that the curves in Figs. 3 and 4 change slightly for different H_2 utilization percentages. However, the optimal current density changes very little. For example, operating at 25% H_2 utilization only shifts the optimal value to 0.45 A cm^{-2}. Therefore, since Fig. 4 shows that system energy density is a relatively weak function of current density near the optimum, it is sufficient for the purposes of this work to assume a constant current density of 0.44 A cm^{-2} in all subsequent calculations.

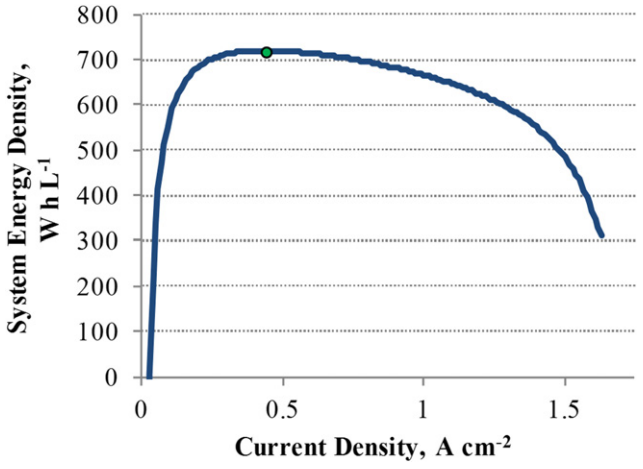

Fig. 4. System energy density v. current density.

3.2. Effects of H_2 utilization and depth

Fig. 5 plots energy density vs. the H_2 utilization of the fuel cell for the two cases described in Section 2.3 assuming adiabatic (lower curves) and isothermal (upper curves) hydrogen compression at 70% adiabatic and isothermal efficiency, respectively. Recall that adiabatic and isothermal compression provide the lower and upper bounds of system performance. Depths ranging from 3 to 150 m are considered in order to span the operating range defined by the Navy for UUVs in this class [23,24]. Case A and B curves converge at 53% utilization where there is no longer any excess H_2 to dispose of.

The figure shows that venting excess H_2 overboard (Case A) leads to higher system-level energy densities than storing (Case B) does. With adiabatic compression at 3 m, Case A delivers a peak energy density of 806 W h L^{-1} at 25% hydrogen utilization. This is 12% higher than the energy density at full (53%) H_2 utilization and 24% higher than at 0% utilization (i.e., 24% better than the baseline HAC system). The peak occurs because of a competition between system efficiency and the displacement of fuel by the fuel cell system. As utilization increases from zero, the HAC system shrinks and the overall cycle efficiency increases because load is shifted to the more efficient fuel cell. As the SOFC grows, however, more volume is consumed by it and the H_2O_2. This decreases the total amount of energy stored on board the vehicle and will eventually outstrip the gains in system efficiency. It should be noted that other factors may make operation at 25% utilization undesirable. The system would have the added complexity of the SOFC without eliminating H_2 venting or delivering a 'game-changing' performance improvement over the baseline HAC. Therefore, it could be more desirable to operate at full H_2 utilization even in cases where venting is permitted.

Using isothermal compression for Case A changes the shape of the energy density curve at low H_2 utilizations, and improves the

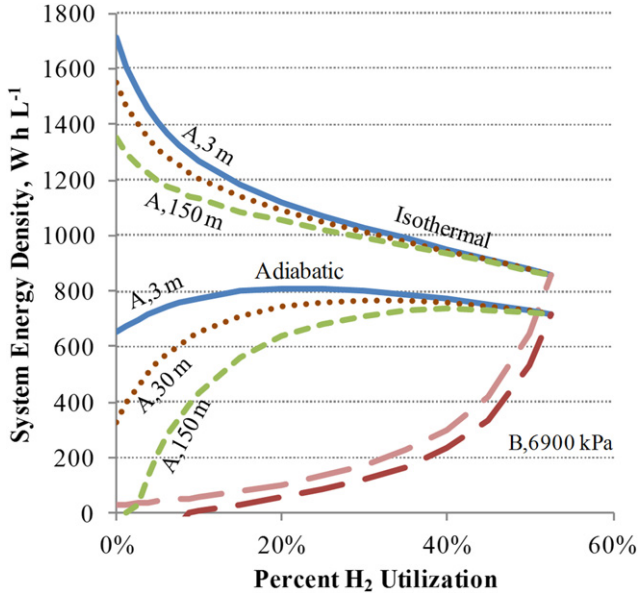

Fig. 5. HAC-SOFC volumetric energy density v. hydrogen utilization.

energy density of the system by more than 150% at 0% H_2 utilization compared to adiabatic compression. The degree of improvement decreases as utilization increases but still yields a 19% improvement in system energy density at full H_2 utilization. These results suggest that increasing complexity using cooled compressors capable of compressing gases isothermally could be very worthwhile. However, these results should be regarded as an upper bound on what is possible as no accounting has been made for the additional volume (such as heat exchangers) that may be required to implement the isothermal compression process.

The effects of increasing vehicle depth are also shown in Fig. 5. As depth is increased, more work is required to raise the hydrogen to the ambient pressure. This causes the system energy density to drop off at greater depths. At 0% H_2 utilization and 150 m depth, more power is required to discharge the H_2 adiabatically than is produced by the system and the cycle is no longer thermodynamically viable. At 53% utilization the energy density of the system becomes nearly depth independent as the different depth curves converge. Therefore, an important benefit of the fuel cell is that it makes the vehicle far more versatile by neutralizing the impact of depth.

Case B with adiabatic compression (to 6900 kPa) shows much worse performance than Case A. System energy density actually becomes negative at H_2 utilizations $< 8\%$ because the volume required for H_2 storage leaves no room for reactants. Using isothermal compression permits operation (i.e., provides a positive energy density) for the pure HAC system (0% utilization) with H_2 storage, but system energy density is still quite low. The Case B curve is essentially independent of depth because storage work is independent of depth and the work to pump in ambient water is negligible relative to other factors.

3.3. Cost of handling excess H_2

In Case A, the work required to compress the hydrogen to ambient (depth) pressure reduces the net output of the system. The impact at a depth of 3 m for both adiabatic and isothermal compression processes is illustrated in Fig. 6. The left bars in each grouping show the gross power output of the system which is the sum of the turbine and SOFC powers. The right bars in each grouping show the losses: H_2 ventilation work, H_2 recirculation work, and water pump work. Subtracting the losses from the total power gives the net power output which is 15 kW for all H_2 utilizations. The figure shows that at maximum H_2 utilization (53%), no work is required to vent because there is no excess hydrogen. The work required to vent is quite large with no SOFC (0% utilization) and adiabatic compression. In addition, because the hydrogen recirculation work is roughly proportional to the turbine work, the losses in the system increase with turbine work leading to increased fuel consumption and plummeting efficiency. This is evident in the figure where the gross work at 0% utilization and adiabatic compression is several times higher than at 53% utilization for the same net power. The figure also illustrates the enormous benefit of compressing isothermally. The gross work required at 0% utilization drops by nearly 60% when the compression is switched to isothermal because the parasitic demand drops by over 75%.

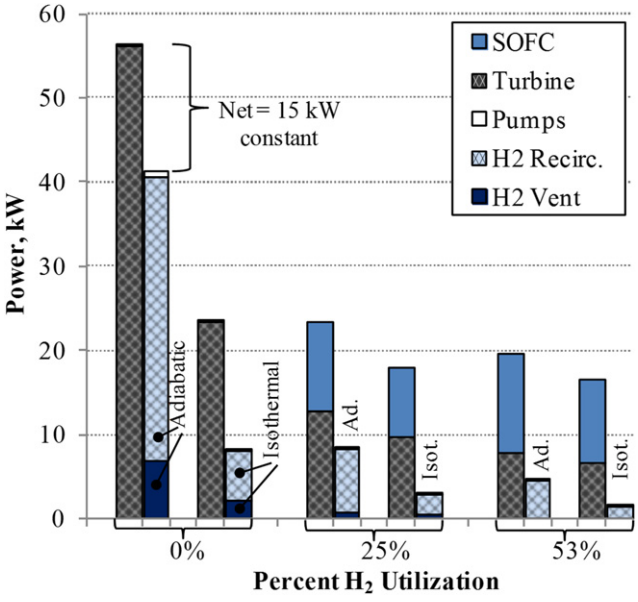

Fig. 6. Case B at 3 m, components of net power.

Storing the excess hydrogen is the alternative to venting, but this also incurs a significant performance penalty. The work required for compression results in the need for larger SOFC and HAC systems to supply the demand. More importantly, the H_2 storage tank itself displaces a large amount of fuel. These larger systems displace fuel and greatly reduce the energy storage capacity of the vehicle. Fig. 7 shows how the fraction of interior volume available for fuel disappears as the utilization decreases and the HAC, SOFC, and H_2 storage dominate. Fig. 7(a) shows that when utilization is less than 8% and the compression process is adiabatic, all of the fuel is displaced and no solution exists that makes physical sense. Fig. 7(b) shows that compressing isothermally removes this restriction and allows the HAC and SOFC to be much smaller than in the adiabatic compression case. However, the H_2 storage volume still dominates at low utilization. It should also be noted that in a 'real' system, the HAC volume will be larger than shown in Fig. 7(b) due to the added volume of the isothermal compressor.

3.4. Sensitivity analysis

A sensitivity analysis is performed to quantify the relative impact of several parameters on the volumetric energy density of the system. This allows a more direct determination of which factors are most important for advancing the technology. The 'sensitivity coefficient' with respect to parameter X (S_X) is defined as the fractional change in system energy density divided by the fractional change in the parameter, as given by Eq. (23) where '*ref*' refers to the baseline assumptions and results and prime values denote the values of the perturbed parameter and the resulting energy density.

$$S_X = \frac{\left(\mathrm{ED}_V' - \mathrm{ED}_{V,\mathrm{ref}}\right)\Big/\mathrm{ED}_{V,\mathrm{ref}}}{\left(X' - X_{\mathrm{ref}}\right)\Big/X_{\mathrm{ref}}} \tag{23}$$

The results of the sensitivity analysis are presented in Fig. 8. 'Zero Ut.' corresponds to Case A for the base HAC system with no SOFC and all excess hydrogen vented adiabatically at depth pressure (3 m). 'Full Ut.' corresponds to the case where all excess hydrogen is consumed by the SOFC. Case B at zero utilization is not included due to poor performance at that condition. These results are only for the adiabatic compression case, but trends are similar for isothermal compression.

The efficiency of the turbine has the largest impact (by far) on energy density and is followed in importance by the compressor efficiency. This is expected because those parameters directly control the system's mechanical power output and the primary parasitic loss, respectively. Therefore, improving η_C and η_T is the

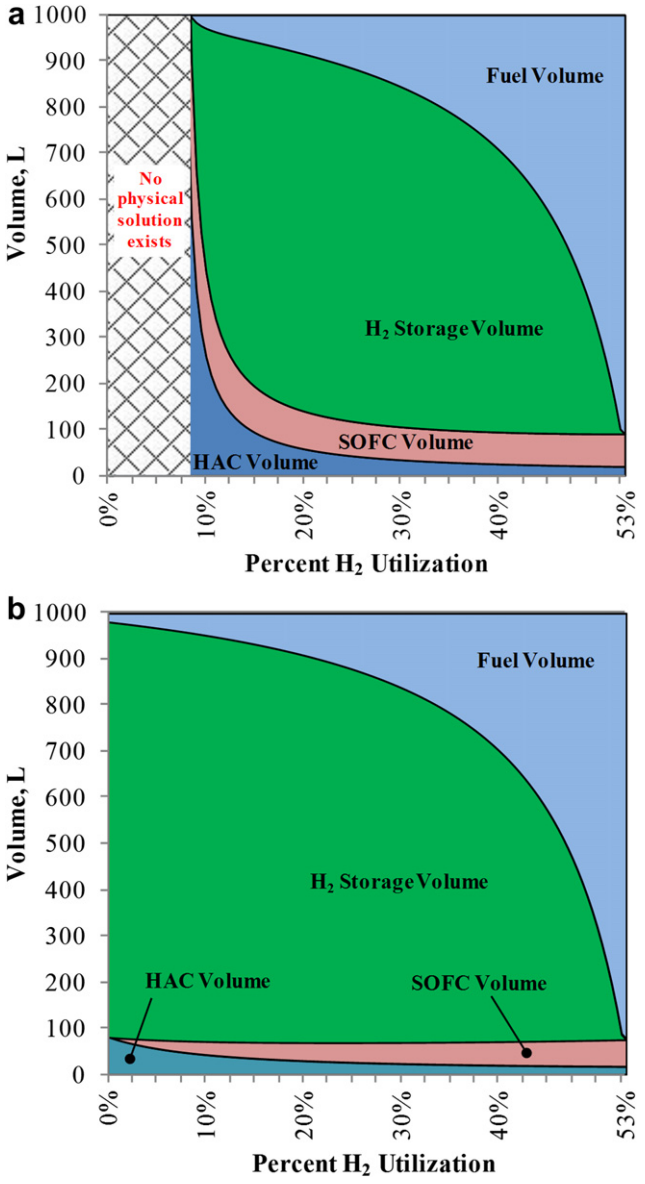

Fig. 7. Case C at 6900 kPa, volume v. H_2 utilization, (a) adiabatic compression, (b) isothermal.

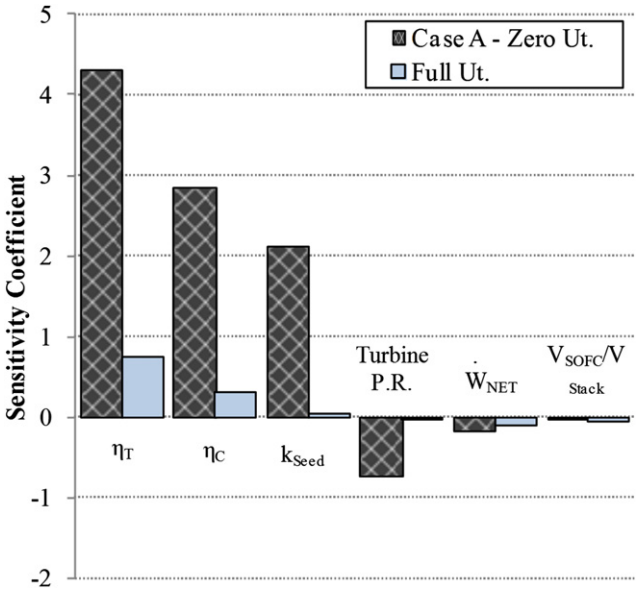

Fig. 8. Sensitivity analysis.

most effective way to raise system energy density. The impact is reduced at full utilization where the SOFC provides a large fraction of the power thereby reducing the overall influence of the HAC portion of the system on overall energy density.

Increasing the seed ratio (or reducing the amount of H_2 required to deliver a particular amount of aluminum from the seeder to the combustor) has a somewhat complex effect on the system. Energy density is increased significantly for Case A at zero utilization because the efficiency of the system is improved by reducing the fraction of H_2 that must be recirculated. However, the improvement is negligible at full utilization. This is because reducing the fraction of H_2 that recirculates reduces the H_2 fraction in the anode flow and forces an increase in H_2 utilization rate by the cell. Both of these changes result in decreased fuel cell efficiency which negates the benefit seen at zero utilization.

Reducing the pressure ratio decreases the work output of the turbine but also decreases the work required to compress the hydrogen by keeping its pressure higher leaving the turbine. This turns out to have a net positive impact on performance. The sensitivity to turbine pressure ratio is small at high utilization rates where the amount of hydrogen to compress is small.

Increasing the net power decreases the energy density of the system. The decrease is expected, and it occurs because of how the components are scaled to meet the power demands: When the power requirement increases, all components must become larger which in turn leaves less and less volume for fuel storage. Designing for a low power system is optimal from the point of view of maximizing overall system energy density.

The effect of the SOFC scaling factor (V_{SOFC}/V_{Stack}) was examined because there is a significant degree of uncertainty in the assumption made earlier that the volume of the SOFC support structure (piping, wiring, etc.) scales as twice the volume of the stack alone. As expected, decreasing the scaling factor raises system energy density because more volume is available for fuel storage. There is no effect at zero utilization because the SOFC is not present, but even at full utilization the impact is much less than other factors. Therefore, while the results show that the SOFC scaling factor is important, the effective energy density of the system is much less sensitive to this parameter than most others investigated in this work.

3.5. Performance comparison

Fig. 9 compares the energy densities of the HAC and HAC-SOFC systems investigated in this work to other UUV power systems based on SOFCs [4], lithium-ion [5,8], lead-acid [9], and alkaline [9] battery systems described in the literature. The 'error' bars on the figure indicate the approximate range of performance that one could expect based on either the results presented above (for the HAC and HAC-SOFC systems) or the reports in the literature. '0% Ut.' represents the base HAC system with no SOFC. 'Full Utilization' represents the case where all excess hydrogen is consumed by the SOFC. The solid bars for the HAC and HAC-SOFC systems correspond to energy densities associated with adiabatic H_2 compression and the baseline assumptions described throughout this work. The top of the cross-hatched bars show the maximum possible system energy density associated with an isothermal compressor, under baseline assumptions, that consumes no additional interior volume

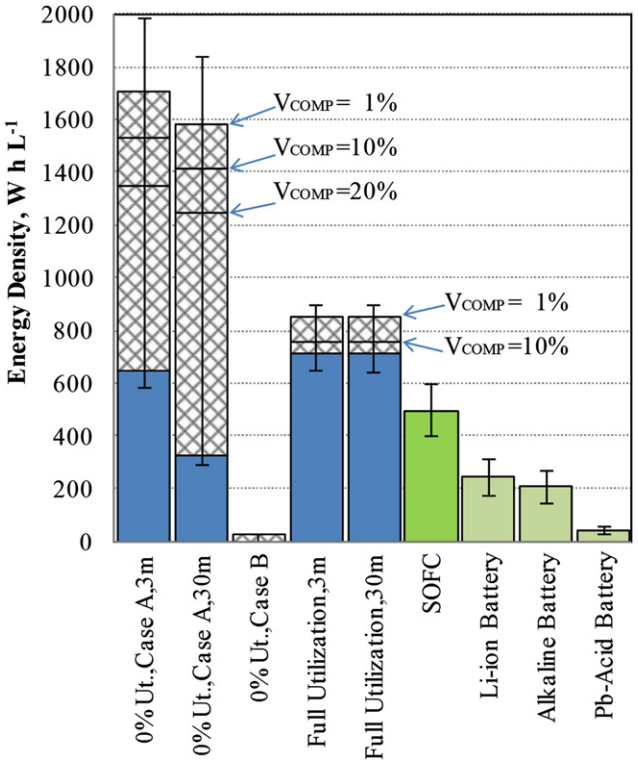

Fig. 9. Bar graph of energy density of various technologies.

compared to an adiabatic compressor. The intermediate lines in the cross-hatched portion show the boundaries associated with isothermal compression systems that consume various fractions (10% and 20%) of the available interior volume. The lower value range bars show an arbitrary 10% decrease in performance that could be attributed to losses that are beyond the scope of the present work to predict (i.e., pressure and thermal losses in plumbing etc.). The upper value range bars for the HAC and HAC-SOFC systems show what levels of performance could be possible if all the improvements investigated in this study were realized.

The results show that for Case A (hydrogen venting) the energy density of the baseline HAC system is at least 2.5 times greater than a lithium-ion battery system and three times greater than an alkaline battery powered system. Improvements by factors of seven to eight are possible if isothermal compression can be successfully implemented. The degree of improvement decreases with increasing depth. The HAC system for Case B (hydrogen storage) has extremely low energy density making it an undesirable option. The HAC-SOFC system running at full H_2 utilization offers a three- to four-fold increase in range over battery systems and achieves depth independence. It also avoids venting gas overboard which can be undesirable for reasons of stealth.

It is clear from Fig. 9 that the level of performance that can be achieved depends strongly on the degree to which isothermal compression can be achieved without incurring large volume penalties. However, a significant improvement in performance is still observed even when 10% (or as high as 20%–30% for the HAC) of the total available volume is dedicated to the isothermal compressor. This suggests that isothermal compression is an attractive option in spite of difficulties that could arise in designing a compact and practical compressor.

As a final note, one might be tempted to dispense with the fuel cell and simply 'burn' the aluminum with the stored peroxide. Earlier work [2], however, has shown that this is not advantageous since the improved thermodynamic efficiency of the fuel cell is no longer available to offset the energy density penalty associated with the stored oxidizer.

4. Conclusions

A model of a novel underwater power system based on the exothermic reaction between seawater and aluminum was developed using the Numerical Propulsion System Simulation system modeling environment. Thermodynamic models were developed for each component of the system and methodologies were developed for estimating their volumes based on the flows of reactants through them. The overall objective was to investigate the efficacy of incorporating a solid oxide fuel cell to consume waste hydrogen produced by the aluminum–water reaction.

The results show that it is always more effective from a volumetric energy density standpoint to vent any excess hydrogen as opposed to storing it. This is because the gas storage tanks displace large amounts of fuel. Likewise, consuming all of the excess hydrogen in the fuel cell of the HAC-SOFC is always more effective than storing it.

When stealth is necessary (i.e., when H_2 venting is not permitted) the HAC-SOFC at "full" utilization is the best option. It provides better energy density than a pure SOFC and up to three to four times better energy density than current battery technology (Li-ion and alkaline). This system avoids the need to vent any gaseous waste products, and it is depth independent. Also, adding the fuel cell could potentially enable periods of silent operation by shutting down the steam turbine and operating on stored H_2.

When stealth is not important, deciding between HAC with H_2 venting and HAC-SOFC depends on the depth profile of the mission and whether or not isothermal compression is achievable. The energy density of the pure HAC system with isothermal compression is more than two times greater than the peak energy density of the HAC-SOFC system. This can provide up to a seven- or eight-fold improvement in system energy density over battery technologies.

Acknowledgments

The authors would like to thank Dr. Joseph Fontaine of the Naval Undersea Warfare Center-Newport Branch, Mr. Tom Lavelle of the NASA Glenn Research Center, and Dr. Greg Jackson of the University of Maryland for their help and guidance, and Ms. Maria Medeiros and the Office of Naval Research for their support of this work under contract N00014-08-1-0717.

References

[1] The Navy Unmanned Undersea Vehicle (UUV) Master Plan, Department of the Navy, 2004.
[2] D.F. Waters, M.S. thesis, University of Maryland, College Park, 2011.
[3] L. Greiner, in: L. Greiner (Ed.), Underwater Missile Propulsion, Compass Publications, Arlington, VA, 1967, pp. 269–279.
[4] A.A. Burke, L.G. Carreiro, J. Power Sources 158 (2006) 428–435.
[5] J.B. Lakeman, A. Rose, K.D. Pointon, D.J. Browning, K.V. Lovell, S.C. Waring, J.A. Horsfall, J. Power Sources 162 (2006) 765–772.
[6] J.A. Peters, Summary of Recent Hybrid Torpedo Powerplant Studies, Pennsylvania State University Applied Research Laboratory, 2007, Technical Report No. 07-004.
[7] M.S. Haberbusch, R.J. Stochl, C.T. Nguyen, A.J. Culler, J.S. Wainright, M.E. Moran, in: Proc. IEEE Workshop Autonomous Underwater Vehicles, San Antonio, 2002, pp. 103–109.
[8] R. Gitzendanner, F. Puglia, C. Martin, D. Carmen, E. Jones, S. Eaves, J. Power Sources 136 (2004) 416–418.
[9] D. Linden, T.B. Reddy, Handbook of Batteries, sixth ed., McGraw-Hill, New York, 2002, p. 1.16.
[10] D.H. Kiely, Joint Propulsion Conference, Indianapolis, IN, June 27, 1994.
[11] W.D. White, in: L. Greiner (Ed.), Underwater Missile Propulsion, Compass Publications, Arlington, VA, 1967, pp. 281–288.
[12] G. Roy, Advances in Chemical Propulsion: Science to Technology, CRC Press, Boca Raton, FL, 2001.

[13] B.H. Carmichael, in: L. Greiner (Ed.), Underwater Missile Propulsion, Compass Publications, Arlington, VA, 1967, pp. 147–169.
[14] T.F. Miller, J.L. Walter, D.H. Kiely, Workshop on Underwater Vehicles, June 20–21, 2002.
[15] W.E. Eagle, D.F. Waters, C.P. Cadou, AIAA Aerospace Sciences Meeting, Nashville, TN, Jan. 9–12, 2012.
[16] W.E. Eagle, M.S. thesis, University of Maryland, College Park, 2007.
[17] D.F. Waters, C.P. Cadou, AIAA-2012-1134, 50th AIAA Aerospace Sciences Meeting, Nashville, TN, Jan. 9–12, 2012.
[18] C.B. Hopson, Joint Propulsion Conference, San Diego, CA. July 10–12, 2005.
[19] U. Bossel, Proc. IEEE 94 (2006) 1826–1837.
[20] E. Tzimas, C. Filiou, S.D. Peteves, J.B. Veyret, Hydrogen Storage: State-of-the-art and Future Perspective, European Commission, Directorate General Joint Research Centre, Institute for Energy, Petten, The Netherlands, 2003.
[21] NPSS User Guide, Software Release 1.6.5, NASA, 2008.
[22] B. McBride, S. Gordon, Computer Program for Calculation of Complex Chemical Equilibrium Compositions and Applications II. User's Manual and Program Description, 1996, NASA Publication RP-1311-P2.
[23] Large Displacement Unmanned Underwater Vehicle Innovative Naval Prototype Energy Section Technology, Office of Naval Research, 2011, BAA #11-028.
[24] Long Endurance Undersea Vehicle Propulsion, Office of Naval Research, 2011, BAA #11-016.
[25] R.J. Kee, H. Zhu, A.M. Sukeshini, G.S. Jackson, Combust. Sci. Technol. 180 (2008) 1207–1244.
[26] H. Zhu, R.J. Kee, J. Power Sources 169 (2007) 315–326.
[27] H. Zhu, R.J. Kee, V.M. Janardhanan, O. Deutschmann, D.G. Goodwin, J. Electrochem. Soc. 152 (2005) A2427–A2440.
[28] H. Zhu, R.J. Kee, J. Power Sources 117 (2003) 61–74.
[29] X. Li, Principles of Fuel Cells, Taylor & Francis Group, New York, 2006.